MRI texture analysis of GRMD dogs using orthogonal moments : a preliminary study.

G Yang, V Lalande, L Chen, N. Azzabou, Thibaut Larcher, J.D de Certaines, H Shu, Jean-Louis Coatrieux

Disponible en ligne sur
ScienceDirect
www.sciencedirect.com
Elsevier Masson France
EM|consulte
www.em-consulte.com
IRBM 36 (2015) 213–219
IRBM

Original article

MRI texture analysis of GRMD dogs using orthogonal moments: A preliminary study

G. Yang [a,d,*], V. Lalande [b,c,d], L. Chen [a,d], N. Azzabou [e], T. Larcher [f], J.D. de Certaines [e], H. Shu [a,d], J.-L. Coatrieux [a,b,c,d]

[a] *Lab of Image Science and Technology – Key Laboratory of Computer Network and Information Integration (Southeast University), Ministry of Education, China*
[b] *INSERM, U1099, Rennes, France*
[c] *Laboratoire de Traitement du Signal et de l'Image, Université de Rennes 1, Rennes, France*
[d] *Centre de Recherche en Information Biomédicale Sino–Français (LIA CRIBs), China–France, France*
[e] *Institut de Myologie, CHU Pitié-Salpêtrière, Paris, France*
[f] *INRA, UMR703 PAnTher, Oniris, Nantes, France*

Received 10 November 2014; received in revised form 15 June 2015; accepted 16 June 2015

Available online 3 July 2015

Abstract

Magnetic resonance image texture analysis (MRI-TA) has been already demonstrated as a powerful tool to extract image information better than visual examination of grey levels. Human muscular dystrophy is a disease of which diagnosis is rather easy but it remains a lack of atraumatic methods for its follow-up as well as for the management of treatments presently in progress. MRI appears to be a potential tool for disease follow-up and treatment monitoring. The present study is part of the European project MYO-MRI (http://myo-mri.eu/) aimed at improving diagnosis and understanding of muscle pathology. This paper focuses on the use of Legendre and Zernike moment-based texture analysis of MRI T2-weighted images to follow from 2 to 14 months 5 healthy and 5 Golden Retriever Muscular Dystrophy Dogs (GRMD), acknowledged to be the most accurate animal model available for human Duchenne Muscular Dystrophy. Regions-Of-Interest (ROIs) were characterized by moments and the features so extracted were analyzed by Principal Component Analysis and classified by means of Support Vector Machine. The preliminary results show relevant discriminations between dogs populations in reference to disease status and evolution.

1. Introduction

The Duchenne muscular dystrophy (DMD), an X-linked recessive disorder, is the most common form of muscular dystrophy. The disease is due to a mutation on the gene coding for dystrophin. The lack of dystrophin makes the membrane unstable, muscle fibers degenerate and are progressively replaced by fibrotic and fat tissue which is mainly responsible for muscular weakness, cardiac dysfunction and death. The Golden Retriever Muscular Dystrophy (GRMD) dog model is acknowledged to be the most accurate model available for DMD and is increasingly used in therapeutic trials [1–3]. The histological expression of the disease closely follows its clinical evolution. The muscle tissue lesions vary according to muscle typography as well as with the age of the dog. Non-invasive follow-up of the disease is to date still problematic. The assessment of positive or deleterious effects of therapies has been conducted with clinical scoring, biochemical studies, muscular strength measurements [4] and particularly with histological examination of biopsies or post-mortem samples. Nevertheless, none of these measurements is completely satisfactory. The use of repeated biopsies might significantly alter the muscle integrity, a critical effect especially in the case of muscular dystrophy study where muscle fibers already undergo degeneration. Furthermore, histological assessment by biopsies, though essential, gives a lim-

* Corresponding author at: Lab of Image Science and Technology, School of Computer Science and Engineering, No. 2 SiPaiLou, Southeast University, 210096, Nanjing, China.
E-mail address: gyyang1980@gmail.com (G. Yang).

http://dx.doi.org/10.1016/j.irbm.2015.06.004
1959-0318/

ited account of the muscle as a whole and therefore might not be representative of what happens in muscle tissue in case of heterogeneity. MRI, for these reasons, is considered a useful tool for non-invasive global evaluation of diseased muscle. The texture of MR images might contain useful information about the state of the muscle tissue. Dystrophic muscle tissue feature such as fibrosis, necrosis and abnormal vascularization could be evaluated by texture analysis (TA). Several successful attempts have already been made to identify abnormal muscle features using MRI [5–13]. In the light of these findings, it appears that MRI-TA could be a powerful image processing tool for a better assessment of diagnosis and therapy effectiveness. A research line in the COST action MYO-MRI (http://myo-mri.eu/) was devoted therefore to explore strategies for muscle imaging texture analysis. Texture methods are classically divided into four categories: structural methods, statistical methods, model-based methods and transform methods (refer for surveys to [14–16]). MRI-TA has been recognized of practical interest in various muscle dysfunctions in MR images of human muscle tissue [17,18], and the detection of muscle lesion in rats [19]. Among the transform group of TA methods, moment-based methods include several families of moments: complex moments, rotational moments, geometric moments and orthogonal moments. Orthogonal moments, such as Legendre and Zernike moments, present the advantage of being optimal with regard to information redundancy [20–22]. Although not yet widely considered in biomedical imaging, moments have already found a few applications for the segmentation in ultrasound images [23], and the discrimination of healthy and disease liver tissue in CT images [24].

The paper is organized as follows. Section 2 defines the protocols and the materials acquired for MYO-MRI. The analysis of the extracted texture features is described as well. Results are reported in Section 3 and discussed in Section 4. The conclusion in Section 5 highlights these preliminary findings and describes the research lines in progress.

2. Materials and methods

2.1. Animals and anaesthesia

The MRI dataset is issued from a longitudinal (2 to 14 months) study of GRMD dogs [11]. Five control and five GRMD dogs were bred in a dedicated gene therapy facility at the Alfort National Veterinary School. All procedures were carried out in accordance with the *Guide for the care and the use of laboratory animals* and approved by the Animal Use and Care Committee of the Veterinary School of Alfort, France, following the European legislation on the use of laboratory animals. The anaesthesia of the dogs was induced by intravenous injection of propofol (RapinovetND, MSD-Schering-Plough, Courbevoie, France) at the dose of 0.65 ml/kg. The dogs were intubated with an endotracheal tube and general anesthesia was maintained using an inhalational mixture of 2% isofluorane (ForeneND, Abbott, Chicago, USA) and oxygen. Body temperature, heart rate and oxygen saturation were constantly monitored (Maglife Odam, Schiller Medical, Wissembourg, France). During anesthesia, dogs were infused with isotonic sodium chloride solution.

During the first months of GRMD life, individual degenerating/necrotic fibers and clusters of regenerating fibers are prominent with numerous hypercontracted fibers also called hyalin fibers, some inflammatory cells and mild endomysial and perimysial fibrosis. Fibrosis later develops with a variable distribution across different muscles. Adipose tissue infiltration can start to occur at four months of age with a variable distribution [2,3]. Clinical function tests have a fast negative evolution from 2–3 to 6 months before a period of paradoxical stability during the next months. According to these histological main variations, disease evolution can be approximately divided in three different periods: phase 1 (0 to 3–4 month) is mainly characterized by degenerating fibers but also regenerating groups, inflammatory cells, hypercontracted cells, beginning of fibrosis and large decrease of clinical functions. Phase 2 (around 4–6 months) is characterized by increased fibrosis, fat infiltration and a relative stability of clinical signs. Fig. 1 shows histological slices of skeletal muscle after specific staining for fibrosis evidencing the tissue changes between phase 1 and phase 2. During phase 3 (from around 6 months up to death), fibrosis and fat infiltration are variable with important prenecrotic and necrotic tissues.

2.2. MR images acquisition

NMR acquisitions were performed at the NMR laboratory of the Institute of Myology, Pitié-Salpétrière University Hospital, using a 3T Siemens Magnetom Trio TIM imager/spectrometer (Siemens Healthcare, Erlangen, Germany) with the standard circularly polarized extremity coil. A T2-weighted (Spin Echo sequence, TR = 3000 ms, TE1 = 6.3 ms, TE2 = 50 ms, NEX = 5, 12–14 axial slices along the limb with a slice thickness of 3 mm and an in-plane resolution of 0.56×0.56 mm^2) was performed. The NMR protocol included T1-weighted and proton density images but according to results obtained by Thibaud et al. [11], the T2-weighted images provided the most promising results in terms of heterogeneity criteria when compared to T1-weighted. The heterogeneity was defined as the standard deviation corrected for noise and it was significantly higher in T2-weighted images of GRMD dogs. Thus, it was assumed that this increase of heterogeneity with disease may be related to the development of a fibrosis that impacts the T2 values. The T1- and T2-weighted images were acquired during the same scanning session, with exactly the same geometrical parameters. The animals were anaesthetized so that no motion correction was needed and no registration step was required.

Fig. 2 displays two sample images of a GRMD dog and a healthy dog with a zoom on one limb. MR images of the GRMD and healthy dogs were acquired every few months (Table 1). Although the acquisitions were not worked out the same month of age due to the facilities constraints, they well match the three phases previously mentioned. Some GRMD dogs died from respiratory complications between 9 and 12 months of age.

Four muscles of the hind limbs (right and left legs) were considered: the *Extensor digitorum longus* (EDL), the *Gastroc-*

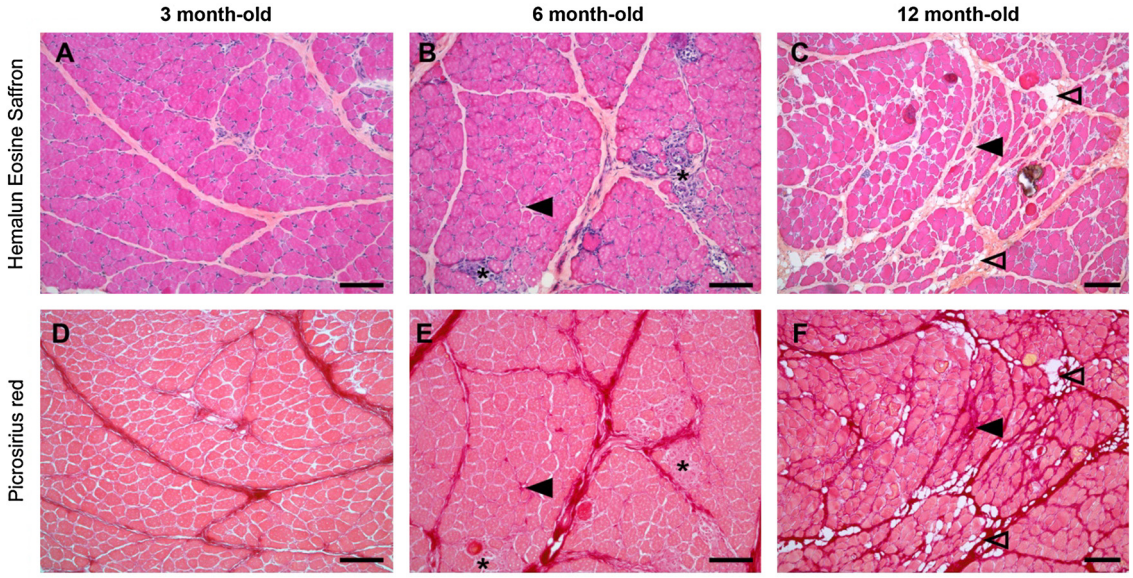

Fig. 1. Typical histopathological presentation of skeletal muscles of GRMD dogs, 3, 6 and 12 month-old. Changes are mild at 2 months (A) with only some hypercontracted fibers, and a diffuse increase in cell number. At 6 months, degenerative and necrotic changes are more severe, elicitating some inflammatory cell infiltration (∗). At 12 months, fibrotic (black arrowhead) and fat tissues (open arrowhead) are proeminent. (A–C) Hemalun eosin saffron and (E–F) Picrosirius red stainings. Bars = 100 μm (A–B, D–E) and 200 μm (C and F). Collagen (fibrosis) is red with Picrosirius staining and yellow with Hemalun eosin saffron staining. (For interpretation of the references to color in this figure legend, the reader is referred to the web version of this article.)

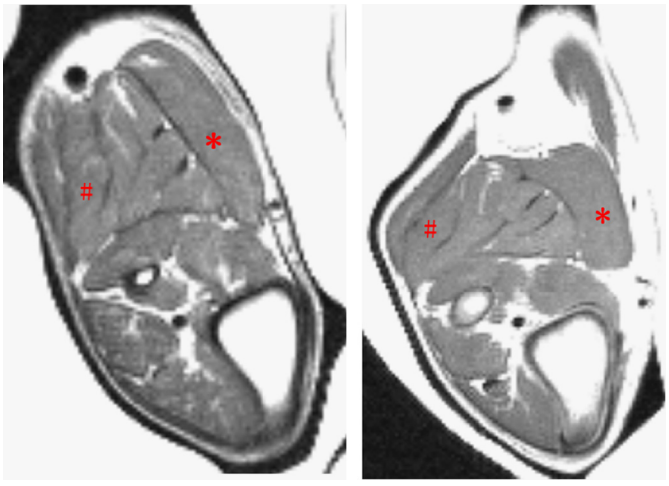

Fig. 2. Examples of T2-weighted MR images in a 4-month-old GRMD dog (left) and a 4-month-old healthy dog (right). The images are zoomed on the right limbs to show the detail of muscles. Two interested muscles for texture analysis in this paper, i.e. GL and GM, are marked by # and ∗ respectively.

nemius lateralis (GL), the *Gastrocnemius medialis* (GM) and the *Tibial cranialis* (TC). Indeed, other muscles are too small for including enough pixels for TA. The ROIs were manually drawn by an MRI specialist, thus composing 936 diseased muscle Regions-Of-Interest (ROI) images of GRMD and 1057 of healthy dogs. The contours were traced on a preliminary T1 Fat Saturated weighted images and transferred on the T2-weighted images. Flow artifact, if any, large vessels and areas of partial volume effects were carefully excluded from the ROIs. Muscles were contoured in all images where they were visible. The ROI sizes depend on the muscle and the position of the slices: in average, there are 90 pixels for the GM and TC, 56 pixels for the GL and 60 pixels for the EDL. In most cases the number of slices available for the delineation of a given muscle ranges from three to eight.

Table 1
Rows indicate the dog's reference, columns the months (M) were MRI acquisitions were performed.

Dataset acquisitions											
	Dog	Age									
		2M	3M	4M	5M	6M	8M	9M	11M	12M	14M
Diseased	1	+		+		+	+				
	2			+	+		+				
	3	+			+			+	+		
	4			+	+		+		+		
	5	+		+		+					
Healthy	6	+	+		+		+				
	7				+		+		+		
	8	+	+		+		+				+
	9	+		+		+	+			+	
	10			+			+		+		

2.3. Image processing and texture analysis methods

The TA methods which has been used in this preliminary study includes the Legendre and the Zernike moments (a comprehensive survey can be found in [20–22] and in-depth information in [25,26]).

2.3.1. Legendre moments

The two-dimensional (2D) $(n+m)$th order of Legendre moment of an image intensity function $f(x, y)$, L_{nm}, is defined as [20]

$$L_{nm} = \frac{(2n+1)(2m+1)}{4} \int_{-1}^{1}\int_{-1}^{1} P_n(x) P_m(y) f(x, y) dx dy, \quad (1)$$

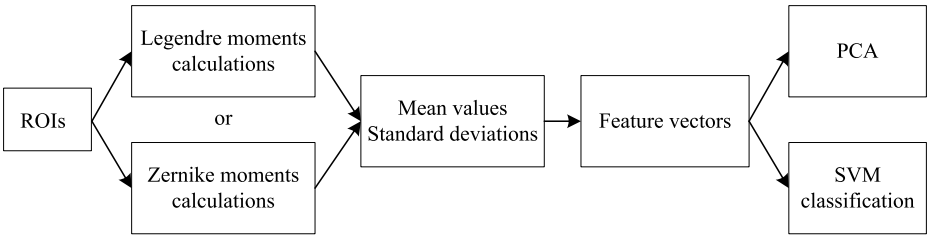

Fig. 3. Global analysis process where "PCA" stands for Principal Component Analysis and "SVM" for Support Vector Machine.

where $P_n(x)$ is the nth order of Legendre polynomial given by

$$P_n(x) = \frac{1}{2^n}\sum_{k=0}^{n/2}(-1)^k \frac{(2n-2k)!}{k!(n-k)!(n-2k)!}x^{n-2k}. \quad (2)$$

Since the Legendre polynomials are orthogonal over the interval $[-1, 1]$, the image $f(x, y)$ can be reconstructed from its moments. Teague [27] derived a simple approximation to the inverse transform for a set of moments through order P given by

$$f(x, y) \approx \sum_{n=0}^{P}\sum_{m=0}^{n} L_{n-m,m}\, P_{n-m}(x)\, P_m(y). \quad (3)$$

When an analog original image is digitized to its discrete form, the 2D Legendre moments L_{nm} defined by Eq. (1) are usually approximated by

$$L_{nm} = \frac{(2n+1)(2m+1)}{(N-1)(M-1)}\sum_{i=1}^{N}\sum_{j=1}^{M} P_n(x_i)\, P_m(y_j)\, f(i, j), \quad (4)$$

with $x_i = \frac{2i-N-1}{N-1}$, $y_i = \frac{2j-M-1}{M-1}$.

2.3.2. Zernike moments

The 2D Zernike moments, Z_{nm}, of order n with repetition m, are defined in polar coordinates (r, θ) inside the unit circle as [20]

$$Z_{nm} = \frac{n+1}{\pi}\int_0^1\int_0^{2\pi} R_{nm}(r)e^{-jm\theta} f(r, \theta) r\, dr\, d\theta,$$
$$0 \le |m| \le n,\ n - |m| \text{ being even.} \quad (5)$$

where $R_{nm}(r)$ is the nth order of Zernike radial polynomial given by

$$R_{nm}(r) = \sum_{k=0}^{(n-|m|)/2} (-1)^k \frac{(n-k)!}{k!\left[(n-2k+|m|)/2\right]!\left[(n-2k-|m|)/2\right]!} r^{n-2k}. \quad (6)$$

Like the rotational moments and the complex moments, the magnitude of the Zernike moments is invariant under image rotation transformation. The image can be reconstructed using a set of moments through order P as

$$f(r, \theta) \approx \sum_{n=0}^{P}\sum_{m} Z_{nm} R_{nm}(r) e^{jm\theta}. \quad (7)$$

Eq. (5) can be discretized as [28]

$$Z_{nm} = \frac{n+1}{\pi(N-1)^2}\sum_{i=1}^{N}\sum_{j=1}^{N} R_{nm}(r_{ij}) e^{-jm\theta_{ij}} f(i, j), \quad (8)$$

where N is the number of pixels along each axis of the image, the mapping transformation to the interior of the unit circle is given by

$$r_{ij} = \sqrt{(c_1 i + c_2)^2 + (c_1 j + c_2)^2},$$
$$\theta_{ij} = \tan^{-1}\left(\frac{c_1 j + c_2}{c_1 i + c_2}\right), \quad (9)$$

with $c_1 = \sqrt{2}/(N-1)$, $c_2 = -1/\sqrt{2}$.

2.4. Feature extraction and data analysis

In order to compare the results obtained by the different groups involved in MRI-TA of MYO-MRI, standard methods for data analysis have been chosen. This is important to determine the role played by the extracted features alone and to decide what features better capture the tissue properties. So, the extracted moment features are examined in a first step by applying a Principal Component Analysis (Fig. 3) and in parallel classified using a Support Vector Machine (SVM) technique. As seen in the equations above, the Legendre and Zernike moments of a function are calculated respectively inside the interval $[-1, 1]$ and the unit circle. In order for the moment to preserve the image information as accurately as possible, ROIs must be placed in appropriate bounding boxes. Several configurations were tested in each case to take into account the varying muscle shapes: (i) by defining the largest bounding box over all ROIs, and centering or not the other ROIs inside, with complementary zero values outside the ROIs; (ii) by selecting the smallest box bounding each ROI with zero values added outside the ROI. Among the all tests performed so far, the second option was retained for the Legendre moments. The same systematic approach was applied for Zernike moments and the best solution was obtained by first setting the minimal square window containing the ROI and then by using the bounding circle with proper zero values inserted accordingly.

The basic set of moments calculated for the study are: Legendre moments LM_{00}, LM_{10}, LM_{01}, LM_{11}, LM_{20}, LM_{02} and Zernike moments ZM_{00}, ZM_{11}, ZM_{20}, ZM_{22}, ZM_{31}, ZM_{33}. Adding higher order up to the third order for Legendre moment values was also tested. The moments are calculated in all 2D ROIs and then gathered for a whole muscle by keeping the

mean moment values over the available slices (six Legendre moments and six Zernike moments). The standard deviations are also calculated and build the second half part of the feature vector. Legendre and Zernike moments are treated separately. Several options were considered depending or not on a normalization of the moment values by LM_{00} and ZM_{00} respectively. They lead either to an 80 feature vector or a 96 feature vector. The feature vectors of the eight muscles are then assembled to form the final feature vector: this vector represents the imaging information corresponding to all muscles of a dog at a certain time. The same approach was applied when considering the third order of Legendre moments.

A descriptive study was performed by means of the Principal Component Analysis (PCA) [29] in order to get a visual representation of the multi-dimensional data (80 to 96 dimensions depending on the type of feature vector) in a reduced dimensional space. It relies on the principle that some of the variables can be correlated, and therefore can be transformed into a smaller amount of variables called principal components. The principal components are a linear combination of the variables. The data can then be projected on the principal components and visualized. PCA is achieved by finding the eigenvectors (principal components) and eigenvalues (principal values, which account for the quantity of information the eigenvector restitutes) of the covariance matrix of the data. The Support Vector Machine (SVM) [30] was then used to classify the multidimensional data in two classes. Considering the small number of datasets, the leave-one-out cross-validation is used to evaluate the performance of the classification. Different kernel functions and parameters are tested in the experiments. The kernel function and parameters are selected when the best results obtained. As a result, the linear and radial basis function (RBF) kernels are adopted when using Legendre and Zernike moment respectively. The penalty parameter c and γ of RBF kernel are set to 2.0 and 0.02 respectively. The SVM classifier is performed via LIBSVM toolbox (version 3.2) [31].[1]

3. Results

The main results obtained with the two TA methods, Zernike and Legendre moments, are presented in Table 2. 1993 ROIs have been analyzed from the 5 healthy dogs and the 5 GRMD. It means that numerous ROIs are from the same dog but concerning different muscles and different MRI slices. In this preliminary study, a potential difference between the *Extensor digitorum longus*, the *Gastrocnemius lateralis*, the *Gastrocnemius medialis* and the *Tibial cranialis* has not been taken into account. As well a potential difference in the disease evolution for the 5 different GRMD has not been the main goal for this preliminary study.

Using Legendre moment, all the healthy dogs are well classified. Results are not so good with Zernike moment where we have about 15% of false positives (corresponding to 2 dogs on 5). With both methods, the early detection of the disease (month 2) was not possible. At the end (month 4) of phase 1 as previously described, a discrimination between GRMD and healthy dogs starts to appear in 2 GRMD on 5 providing a global sensitivity of about 50% with both methods. Legendre moment method provides a sensitivity of 100% during months 5, 6 and 8 corresponding to the phase 2 of disease evolution; the sensitivity with Zernike method is not so good during this phase 2 with one GRMD determining 57 false negative ROIs. MRI-TA is not a relevant method for early diagnosis easily performed by clinical examination; then, sensitivity appears more relevant than specificity for a-traumatic disease follow-up and evaluation of treatment efficiency. As T2-weighted images can be related to fibrosis, an early modification of MRI-TA parameters is not observed during the first months of evolution but a significant evolution is observed during the second phase of disease evolution as previously described. The last phase of the disease evolution (from 9 month up to death) again provides, as the last phase 1, irregular results. The best results obtained throughout all the tests performed were obtained with the 96 feature vector of Legendre moments which includes the first moment, LM_{00}. The same procedure, conducted with Zernike moments (here also using a normalization of moment values by ZM_{00}) leads to a much complex mixed picture of the two populations and a higher rate of misclassification.

Table 2
Results for Legendre moments (up to the second order) and for Zernike moments (up to the third order). The specificity is the ratio between true negative and condition negative and the sensitivity the ratio between true positive and the condition positive.

AGE (month)	2	3	4	5	6	8	> 9
Healthy ROIs analyzed	111	105	115	144	44	308	230
Diseased ROIs analyzed	121	0	228	161	117	165	144
Sensitivity (Legendre moment)%	0	–	48	100	100	100	34
Specificity (Legendre moment)%	100	100	100	100	100	100	100
Sensitivity (Zernike moment)%	0	–	48	100	48	100	34
Specificity (Zernike moment)%	100	100	100	38	100	40	100

4. Discussion

Despite the fact that the inter-animal variations are large, this first attempt in analyzing the two dog populations is encouraging. These preliminary results show that: i) the different texture parameters do not provide the same sensitivity and specificity; ii) the texture parameters are modified during the disease evolution, iii) the best performance is achieved when using Legendre moments. Another study conducted in parallel in MYO-MRI was based on well-known methods [32] and it was shown that, if the results differed between muscles, among the top methods were the co-occurrence matrix-based, gray-level differences matrix-based, gradient-based, histogram-based, Laws' filtering, and run-length matrix-based. The features from the first method were top ranked for the early stage of GRMD development, while the last method ensured the best tissue recognition for the final stage of canine life [33]. The comparison of different TA methods on the same MRI data, a goal of the European COST action MYO-MRI appears yet to be a relevant challenge not up to now realized by any research consortium.

[1] http://www.csie.ntu.edu.tw/~cjlin/libsvm/.

The second preliminary conclusion suggested by this study opens the discussion on the relationship between MRI-TA and histology though there is a scale gap between the spatial resolutions in clinical MRI and in optical microscopy; for instance, the good sensitivity of Legendre moment method during the phase 2 of the disease suggests a correlation between this MRI-texture parameter and fibrosis. To not use MRI-TA as a "black box" for clinicians, such study has to be performed at a large scale, which is another goal of the European COST action MYO-MRI.

However, the size of the dataset must be extended before arriving to a definitive conclusion on the capability of texture parameters to not only separate the two populations but also track the disease evolution and ultimately follow an effect of treatment. A next step will have to focus on muscle entities in order to understand which muscle is more sensitive to the disease evolution, in what extent it is affected and if it is possible to better characterize the underlying histological processes.

On the methodological side, several issues pointed out by this study must be addressed in the future. Over all the experiments performed so far, the effect of the bounding box has to be better understood. Different bounding boxes have been considered among which a window preset on the largest ROI of a given muscle and a window as small as possible centered on the center of mass of the ROI; they lead to different performances in terms of classification. Another major issue concerns the respective roles of texture, shape, orientation and size of ROIs. The relative impact of these factors is hard to evaluate and both theoretical developments and simulations should be conducted. Increasing the moment orders may provide more details on texture but biases due to noise and the small ROI sizes may limit the significance of higher moment values. Moment invariants [34,35] rather than moments are of interest here since moment invariants are not affected by the position, orientation or scale of the objects.

5. Conclusion

The positive results of the analysis performed in this preliminary study open exciting perspectives in the use of these MRI-TA methods for the follow-up of muscle dystrophy. However, several major questions remain open at the experimental level. From the methodological point of view, several issues have been raised that need further theoretical studies and in particular the analysis of the bounding box effect, the respective roles of texture, shape and orientation of muscle ROIs, the determination of the optimal order of moments to be chosen, the more appropriate kernel functions, etc. However, a systematic exploration of all these factors leads to a very high combinatorial space. Local texture analysis must also be considered: its advantage is to partially avoid the problems related to bounding box selection, ROI shape and orientation mentioned above but with a severe restriction on the number of window samples in each muscle due to the very small sizes of ROIs.

Since about twenty years, a lot of very exciting and positive results of MRI-TA have been published in numerous clinical situations though comparison between various TA methods and explanation of the results in terms of potential histological texture are still in their infancy; it is a major challenge of which the European COST Action MYO-MRI tried to contribute.

Acknowledgements

This research was supported by Chinese National Natural Science Foundation (grants 81101104 and 61271312), National Basic Research Program of China (grant 2011CB707904) and Natural Science Foundation of Jiangsu Province (BK2012743). It has been realized under the auspices of the European Union COST action BM 1304 MYO-MRI.

References

[1] Shelton GD, Engvall E. Canine and feline models of human inherited muscle diseases. Neuromuscul Disord 2005;15(2):127–38.
[2] Valentine BA, Cooper BJ, de Lahunta A, O'Quinn R, Blue JT. Canine X-linked muscular dystrophy. An animal model of Duchenne muscular dystrophy: clinical studies. J Neurol Sci 1988;1(3):69–81.
[3] Nguyen F, Guigand L, Goubault-Leroux I, Wyers M, Cherel Y. Microvessel density in muscles of dogs with golden retriever muscular dystrophy. Neuromuscul Disord 2005;15(2):154–63.
[4] Kornegay JN, Bogan DJ, Bogan JR, Childers MK, Cundiff DD, Petroski GF, et al. Contraction force generated by tarsal joint flexion and extension in dogs with golden retriever muscular dystrophy. J Neurol Sci 1999;166(2):115–21.
[5] Thibaud JL, Monnet A, Bertoldi D, Barthélémy I, Blot S, Carlier PG. Characterization of dystrophic muscle in golden retriever muscular dystrophy dogs by nuclear magnetic resonance imaging. Neuromuscul Disord 2007;17(7):575–84.
[6] Murphy WA, Totty WG, Carroll JE. MRI of normal and pathologic skeletal muscle. Am J Roentgenol 1986;146:565–74.
[7] Leroy-Willig A, Willig TN, Henry-Feugeas MC, et al. Body composition determined with MR in patients with Duchenne muscular dystrophy, spinal muscular atrophy, and normal subjects. Magn Reson Imaging 1997;15:737–44.
[8] Liu GC, Jong YJ, Chiang CH, Jaw TS. Duchenne muscular dystrophy: MR grading system with functional correlation. Radiology 1993;186:475–80.
[9] Matsumura K, Nakano I, Fukuda N, Ikehira H, Tateno Y, Aoki Y. Proton spin-lattice relaxation time of Duchenne dystrophy skeletal muscle by magnetic resonance imaging. Muscle Nerve 1988;11:97–102.
[10] Huang Y, Majumdar S, Genant HK, et al. Quantitative MR relaxometry study of muscle composition and function in Duchenne muscular dystrophy. J Magn Reson Imaging 1994;4:59–64.
[11] Thibaud JL, Azzabou N, Barthelemy I, Fleury S, Cabrol L, Blot S, et al. Comprehensive longitudinal characterization of canine muscular dystrophy by serial NMR imaging of GRMD dogs. Neuromuscul Disord 2012;22(2):S85–99.
[12] Fan Z, Wang J, Ahn M, Shiloh-Malawsky Y, Chahin N, Elmore S, et al. Characteristics of magnetic resonance imaging biomarkers in a natural history study of golden retriever muscular dystrophy. Neuromuscul Disord 2014;24(2):178–91.
[13] Wang J, Fan Z, Vandenborne K, Walter G, Shiloh-Malawsky Y, An H, et al. A computerized MRI biomarker quantification scheme for a canine model of Duchenne muscular dystrophy. Int J Comput Assisted Radiol Surg 2013;8(5):763–74.
[14] Hajek M, Dezortova M, Materka A, Lerski RA, editors. Texture analysis for magnetic resonance imaging. Prague: Med4Publishing; 2006.
[15] Tuceryan M, Jain AK. Texture analysis. In: Chen CH, Pau LF, Wang PSP, editors. Handbook of pattern recognition and computer vision. 2nd edition. World Scientific Publishing Co.; 1998. p. 207–48.
[16] Castellano G, Bonilha L, Li LM, Cendes F. Texture analysis of medical images. Clin Radiol 2004;59:1061–9.

[17] Škoch A, Jirák D, Vyhnanovská P, Dezortová M, Fendrych P, Rolencová E, et al. Classification of calf muscle MR images by texture analysis. Magma 2004;16(6):259–67.
[18] Herlidou S, Rolland Y, Bansard JY, Le Rumeur E, de Certaines JD. Comparison of automated and visual texture analysis in MRI: characterization of normal and diseased skeletal muscle. Magn Reson Imaging 1999;17:1393–7.
[19] Mahmoud-Ghoneim D, Cherel Y, Lemaire L, de Certaines JD, Maniere A. Texture analysis of magnetic resonance images of rat muscles during atrophy and regeneration. Magn Reson Imaging 2006;24(2):167–71.
[20] Shu H, Luo L, Coatrieux JL. Moment-based approaches in imaging, part 1. Basic features. IEEE Eng Med Biol Mag 2007;26(5):70–4.
[21] Shu H, Luo L, Coatrieux JL. Moment-based approaches in imaging, part 2. Invariance. IEEE Eng Med Biol Mag 2008;27(1):81–3.
[22] Shu H, Luo L, Coatrieux JL. Moment-based approaches in imaging, part 3. Computational considerations. IEEE Eng Med Biol Mag 2008;27(3):89–91.
[23] Dos Santos Filho E, Yoshizawa M, Tanaka A, Saijo Y, Iwamoto T. Moment-based texture segmentation of luminal contour in intravascular ultrasound images. J Med Ultrason 2005;32(3):91–9.
[24] Subbiah Bharathi V, Ganesan L. Orthogonal moments based texture analysis of CT liver images. Pattern Recognit Lett 2008;29(3):1868–72.
[25] Mukundan R, Ramakrishnan KR. Moment functions in image analysis—theory and applications. Singapore: World Scientific; 1998.
[26] Flusser J, Suk T, Zitová B. Moments and moment invariants in pattern recognition. New York, NY, USA: Wiley; 2009.
[27] Teague MR. Image analysis via the general theory of moments. J Opt Soc Am 1980;70(8):920–30.
[28] Chong CW, Raveendran P, Mukundan R. Translation invariants of Zernike moments. Pattern Recognit 2003;36(8):1765–73.
[29] Jolliffe IT. Principal component analysis. New York: Springer; 2002.
[30] Cortes C, Vapnik VN. Support-vector networks. Mach Learn 1995;20(3):273–97.
[31] Chang CC, Lin CJ. LIBSVM: a library for support vector machines. ACM Trans Intell Syst Technol 2011;2(3):1–27.
[32] Duda D. Classification d'images médicales basée sur l'analyse de texture. PhD thesis. University of Rennes; 2009.
[33] Lamarque G, Duda D, Bezy J. Unpublished data.
[34] Zhang J, Tan T. Brief review of invariant texture analysis methods. Pattern Recognit 2002;35:735–47.
[35] Shu HZ, Luo LM, Coatrieux JL. Derivation of moment invariants (Book chapter). In: Papakostas GA, editor. Moments and moment invariants: theory and applications. Science Gate Publishing; 2014. p. 57–90.